Physics Letters B 752 (2016) 76–83

Contents lists available at ScienceDirect

Physics Letters B

www.elsevier.com/locate/physletb

Gluon saturation and Feynman scaling in leading neutron production

F. Carvalho [a], V.P. Gonçalves [b], D. Spiering [c], F.S. Navarra [c,*]

[a] Departamento de Ciências Exatas e da Terra, Universidade Federal de São Paulo, Campus Diadema, Rua Prof. Artur Riedel, 275, Jd. Eldorado, 09972-270, Diadema, SP, Brazil
[b] High and Medium Energy Group, Instituto de Física e Matemática, Universidade Federal de Pelotas, Caixa Postal 354, 96010-900, Pelotas, RS, Brazil
[c] Instituto de Física, Universidade de São Paulo, C.P. 66318, 05315-970 São Paulo, SP, Brazil

ARTICLE INFO

Article history:
Received 4 August 2015
Received in revised form 20 October 2015
Accepted 7 November 2015
Available online 11 November 2015
Editor: J.-P. Blaizot

Keywords:
Quantum chromodynamics
Leading particle production
Saturation effects

ABSTRACT

In this paper we extend the color dipole formalism for the study of leading neutron production in $e+p\to e+n+X$ collisions at high energies and estimate the related observables which were measured at HERA and could be analyzed in future electron–proton (ep) colliders. In particular, we calculate the Feynman x_F distribution of leading neutrons, which is expressed in terms of the pion flux and the photon–pion total cross section. In the color dipole formalism, the photon–pion cross section is described in terms of the dipole–pion scattering amplitude, which contains information about the QCD dynamics at high energies and gluon saturation effects. We consider different models for the scattering amplitude, which have been used to describe the inclusive and diffractive ep HERA data. Moreover, the model dependence of our predictions with the description of the pion flux is analyzed in detail. We demonstrate the recently released H1 leading neutron spectra can be described using the color dipole formalism and that these spectra could help us to observe more clearly gluon saturation effects in future ep colliders.

1. Introduction

In high energy collisions the outgoing baryons which have large fractional longitudinal momentum ($x_L \geq 0.3$) and the same valence quarks (or at least one of them) as the incoming particles are called leading particles (LP). The momentum spectra of leading particles have been measured already some time ago [1,2]. Very recently, high precision data on leading neutrons produced in electron–proton reactions at HERA at high energies became available [3].

Leading neutron production is a very interesting process. In spite of more than ten years of intense experimental and theoretical efforts, the x_L (Feynman momentum) distribution of leading neutrons remains without a satisfactory theoretical description [5,4,6–13]. Monte Carlo studies, using standard deep inelastic scattering (DIS) generators show [3,14] that these processes have a rate of neutron production a factor of three lower than the data and produce a neutron energy spectrum with the wrong shape, peaking at values of x_L below 0.3. In order to fit the data the existing models need to combine different ingredients including pion exchange, reggeon exchange, baryon resonance excitation and decay and independent fragmentation [9–13]. Moreover, the incoming photon interacts with the pion emitted by proton and then rescatters, interacting also with the emerging neutron and giving origin to significant absorptive corrections, which are difficult to calculate [10–13]. As it can be seen in Fig. 1, this process is essentially composed by a soft pion (or reggeon) emission and by the subsequent photon–pion interaction at high energies. Pion emission has been studied for a long time and according to the traditional wisdom it can be described by a simple interaction Lagrangian of the form $g\bar{\psi}\gamma_5\pi\psi$, where ψ and π are the nucleon and pion field respectively. The corresponding pion–nucleon amplitude must be supplemented with a form factor, which represents the extended nature of hadrons and at the same time regularizes divergent integrals. The precise functional form of the form factor is very hard (if not impossible) to extract from first principle calculations. We must then resort to models. Very recently [15,16] it has been argued that the Lagrangian which is more consistent with the chiral symmetry requirements is the one with a pseudovector coupling. One of the goals of the present study is to test in a new context the better founded splitting function, $f(y)$, derived in [15]. Additionally, forward hadron production is very important also for cosmic ray physics, where highly energetic protons reach the top of the atmosphere and undergo successive high energy scatterings off light nuclei in the air. In each of these collisions, a projectile

* Corresponding author.
E-mail address: navarra@if.usp.br (F.S. Navarra).

http://dx.doi.org/10.1016/j.physletb.2015.11.017

proton (the leading baryon) looses energy, creating showers of particles, and goes to the next scattering. The interpretation of cosmic ray data depends on the accurate knowledge of the leading baryon momentum spectrum and its energy dependence. A crucial question of practical importance is the existence or non-existence of the Feynman scaling, which says that the x_L spectra of secondaries are energy independent. In cosmic ray applications we are sensitive essentially to the large x_L region (the fragmentation region), which probes the low Bjorken-x component of the target wave function. In this kinematical range nonlinear effects are expected to be present in the description of the QCD dynamics (for recent reviews see [17]), associated to the high parton density. The state-of-art framework to treat QCD at high energies is the Color Glass Condensate (CGC) formalism [18], which predicts gluon saturation at small-x, with the evolution with the energy being described by an infinite hierarchy of coupled equations for the correlators of Wilson lines – the Balitsky–JIMWLK hierarchy [17]. In the mean field approximation, this set of equations can be approximated by the Balitsky–Kovchegov (BK) equation [19,20], which describes the evolution of the dipole-target scattering amplitude with the rapidity $Y = \ln(1/x)$.

In this paper we propose to treat the leading neutron production at HERA using the color dipole formalism, which is able to describe the inclusive and diffractive HERA ep data. Our goal is to extend this successful formalism, which has its main parameters well determined, to leading neutron production. Moreover, the use of the color dipole formalism allows to estimate the contribution of gluon saturation effects to leading neutron production in the kinematical range which was probed by HERA and which will probed in future electron–proton colliders. Finally, it allows to investigate the relation between Feynman scaling (or its violation) and the description of the QCD dynamics at high energies. It is important to emphasize that, in the near future, Feynman scaling will be investigated experimentally at the LHC by the LHCf Collaboration [21–23].

This paper is organized as follows. In the next Section we present a brief review of leading neutron production in ep collisions and the different models for the pion flux are discussed as well. Moreover, the treatment of the process using the color dipole formalism is presented and the main assumptions are analyzed. In Section 3 we analyze the dependence of our predictions on the pion flux and on the scattering amplitude. A comparison with the recent H1 data is presented and Feynman scaling is discussed. Finally, in Section 4 we summarize our main conclusions.

2. Leading neutron production in the color dipole formalism

2.1. The cross section

Let us review the main formulas of leading neutron production. At high energies, this scattering can be seen as a set of three factorizable subprocesses (see Fig. 1): i) the photon fluctuates into a quark–antiquark pair (the color dipole), ii) the color dipole interacts with the pion emitted by the incident proton, and iii) the leading neutron is formed. The differential cross section reads:

$$\frac{d^2\sigma(W, Q^2, x_L, t)}{dx_L dt} = f_{\pi/p}(x_L, t)\sigma_{\gamma^*\pi}(\hat{W}^2, Q^2) \tag{1}$$

where Q^2 is the virtuality of the exchanged photon and $\hat{W}$ is the center-of-mass energy of the virtual photon–pion system. It can be written as $\hat{W}^2 = (1 - x_L)W^2$, where W is the center-of-mass energy of the virtual photon–proton system. As it can be seen in Fig. 1, x_L is the proton momentum fraction carried by the neutron and t is the square of the four-momentum of the exchanged pion.

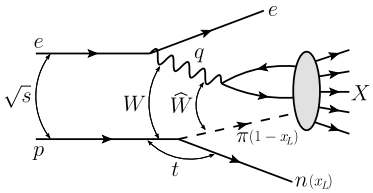

Fig. 1. Leading neutron n production in $ep \to enX$ interactions at high energies. x_L is momentum fraction of the proton carried by the neutron n.

In terms of the measured quantities x_L and transverse momentum p_T, the pion virtuality is:

$$t \simeq -\frac{p_T^2}{x_L} - \frac{(1 - x_L)(m_n^2 - m_p^2 x_L)}{x_L} \tag{2}$$

The flux of virtual pions emitted by the proton is represented by $f_{\pi/p}$ and $\sigma_{\gamma^*\pi}(\hat{W}^2, Q^2)$ is the cross section of the interaction between the virtual-photon and the virtual-pion at center-of-mass energy $\hat{W}$.

2.2. The pion flux

The pion flux $f_{\pi/p}(x_L, t)$ (also called sometimes pion splitting function) is the virtual pion momentum distribution in a physical nucleon (the bare nucleon plus the "pion cloud"). It was first calculated in the early studies [24] of deep inelastic scattering (DIS), where a pseudoscalar nucleon–pion–nucleon vertex was added to the standard DIS diagram. These early calculations were further refined in Refs. [25,26] and even extended to the strange and charm sector [27]. Since pion emission is a nonperturbative process, once we depart from the single nucleon state, we should consider a whole tower of meson–baryon states, having to deal with a series for which there is no rigorous truncation scheme. This led some authors to use light cone models [28] for the pion momentum distribution, where the dynamical origin of the pion is not mentioned and one tries to determine phenomenologically the relative weight of the higher Fock states.

In all the calculations of the pion flux a form factor was introduced to represent the non-pointlike nature of hadrons and hadronic vertices, which contain a cut-off parameter determined by fitting data. The most frequently used parametrizations of the pion flux [5,4,6–13] have the following general form:

$$f_{\pi/p}(x_L, t) = \frac{1}{4\pi}\frac{2g_{p\pi p}^2}{4\pi}\frac{-t}{(t - m_\pi^2)^2}(1 - x_L)^{1-2\alpha(t)}[F(x_L, t)]^2 \tag{3}$$

where $g_{p\pi p}^2/(4\pi) = 14.4$ is the $\pi^0 pp$ coupling constant, m_π is the pion mass and $\alpha(t)$ will be defined below. The form factor $F(x_L, t)$ accounts for the finite size of the nucleon and pion. We will consider the following parametrizations of the form factor:

$$F_1(x_L, t) = \exp\left[R^2\frac{(t - m_\pi^2)}{(1 - x_L)}\right] \quad , \quad \alpha(t) = 0 \tag{4}$$

from Ref. [5], where $R = 0.6$ GeV^{-1}.

$$F_2(x_L, t) = 1 \quad , \quad \alpha(t) = \alpha(t)_\pi \tag{5}$$

from Ref. [4], where $\alpha_\pi(t) \simeq t$ (with t in GeV^2) is the Regge trajectory of the pion.

$$F_3(x_L, t) = \exp\left[b(t - m_\pi^2)\right] \quad , \quad \alpha(t) = \alpha(t)_\pi \tag{6}$$

from Ref. [6], where $b = 0.3$ GeV^{-2}.

$$F_4(x_L,t)=\frac{\Lambda_m^2-m_\pi^2}{\Lambda_m^2-t}\quad,\quad \alpha(t)=0 \tag{7}$$

from Ref. [7], where $\Lambda_m=0.74$ GeV.

$$F_5(x_L,t)=\left[\frac{\Lambda_d^2-m_\pi^2}{\Lambda_d^2-t}\right]^2\quad,\quad \alpha(t)=0 \tag{8}$$

also from Ref. [7], where $\Lambda_d=1.2$ GeV. In the case of the more familiar exponential (4), monopole (7) and dipole (8) forms factors, the cut-off parameters have been determined by fitting low energy data on nucleon and nuclear reactions and also data on deep inelastic scattering and structure functions.

In all analyses of pion cloud effects in DIS the authors have used pseudoscalar (PS) coupling, which is, by itself, inconsistent with chiral symmetry. More recently, in [15] the authors used an effective chiral Lagrangian for the interaction of pions and nucleons consistent with chiral symmetry. Unlike the earlier chiral effective theory calculations which only computed the light-cone distributions of pions or considered the non-analytic behavior of their moments to lowest order in the pion mass, in [15] the authors have computed the complete set of diagrams relevant for DIS from nucleons dressed by pions resulting from their Lagrangians, without taking the heavy baryon limit. In particular, they have demonstrated explicitly the consistency of the computed distribution functions with electromagnetic gauge invariance. In [16] they applied the previously computed pion distribution to the study of the $\bar{d}$–$\bar{u}$ asymmetry in the nucleon. For our purposes, the relevant contribution of the pion momentum distribution reads [15]:

$$f_{\pi/p}(y)=\frac{g_A^2m_n^2}{(4\pi f_\pi)^2}\int_0^{\Lambda_c^2}dp_T^2\,\frac{y(p_T^2+y^2m_n^2)}{[p_T^2+y^2m_n^2+(1-y)m_\pi^2]^2} \tag{9}$$

where $y=1-x_L$, $g_A=1.267$ is the nucleon axial charge, $f_\pi=93$ MeV and $\Lambda_c=0.2$ GeV. In order to obtain the final cross section we multiply (9) by 2 (see [15,16]) and insert it into (1) after integrating the latter over t (or over p_T).

In what follows, we shall use the pion fluxes listed above, in equations (4)–(9), denoting them by f_1, $f_2,\ldots,f_6$, respectively. The main purpose of our calculation will be to show that the dipole approach gives a good description of data and the pion flux is just one element of the calculation. Therefore we will make no effort to choose one particular form. Nevertheless, we note that one important phenomenological constraint that these pion fluxes must satisfy is to reproduce the $\bar{d}$–$\bar{u}$ asymmetry in the proton sea measured by the E866 Collaboration [29]. Among the pion fluxes mentioned above only (8) (see [30]) and (9) have been confronted with these data. As it will be seen later, the results discussed here are very sensitive to the choice of the pion flux and hence leading neutron spectra may be used to constrain its shape.

Before closing this subsection we would like to mention that the diagram shown in Fig. 1 represents only the dominant contribution to leading neutron production. Other isovector meson exchanges, such as ρ or a_2, can also contribute to the leading neutron spectrum. Moreover the $p\to\Delta$ transition can also contribute to neutron production through the subsequent decay $\Delta\to n\pi$. Theoretical studies show that processes other than direct pion exchange are expected to give a contribution of less than 25% of the cross section [5–8,31]. The effect of this background to the one pion exchange is to increase the rate of neutron production. However this effect is partially compensated by the absorptive rescattering of the neutron, which decreases the neutron rate [10–13]. The absorptive corrections are usually represented by a factor K which multiplies the uncorrected cross section of leading neutron production. This factor has a weak dependence on x_L and we shall consider it as a constant.

2.3. The photon–pion cross section

In order to obtain the photon–pion cross section we will use the color dipole formalism, as usually done in high energy deep inelastic scattering off a nucleon target. In this formalism, the cross section is factorized in terms of the photon wave functions Ψ, which describes the photon splitting in a $q\bar{q}$ pair, and the dipole–pion cross section $\sigma_{d\pi}$. We have

$$\sigma_{\gamma^*\pi}(\hat{x},Q^2)=\int_0^1 dz\int d^2\boldsymbol{r}\sum_{L,T}\left|\Psi_{T,L}(z,\boldsymbol{r},Q^2)\right|^2\sigma_{d\pi}(\hat{x},\boldsymbol{r}) \tag{10}$$

where

$$\hat{x}=\frac{Q^2+m_f^2}{\hat{W}^2+Q^2}=\frac{Q^2+m_f^2}{(1-x_L)W^2+Q^2} \tag{11}$$

is the scaled Bjorken variable and the variable $\boldsymbol{r}$ defines the relative transverse separation of the pair (dipole). Moreover, the photon wave functions are given by

$$|\psi_L(z,\boldsymbol{r})|^2=\frac{3\alpha_{em}}{2\pi^2}\sum_f e_f^2 4Q^2z^2(1-z)^2K_0^2(\epsilon r) \tag{12}$$

$$|\psi_T(z,\boldsymbol{r})|^2=\frac{3\alpha_{em}}{2\pi^2}\sum_f e_f^2\left\{[z^2+(1-z)^2]\epsilon^2K_1^2(\epsilon r)+m_f^2K_0^2(\epsilon r)\right\} \tag{13}$$

for a longitudinally (L) and transversely (T) polarized photon, respectively. In the above expressions $\epsilon^2=z(1-z)Q^2+m_f^2$, K_0 and K_1 are modified Bessel functions and the sum is over quarks of flavor f with a corresponding quark mass m_f. As usual z stands for the longitudinal photon momentum fraction carried by the quark and $1-z$ is the longitudinal photon momentum fraction of the antiquark.

The main input in the calculations of $\sigma_{\gamma^*\pi}$ is the dipole–pion cross section. In what follows, for simplicity, we will assume the validity of the additive quark model, which allows us to relate $\sigma_{d\pi}$ with the dipole–proton cross section, usually probed in the typical inclusive and exclusive processes at HERA. Basically, we will assume that

$$\sigma_{d\pi}(x,\boldsymbol{r})=R_q\cdot\sigma_{dp}(x,\boldsymbol{r}) \tag{14}$$

where $R_q=2/3$ is the ratio between the number of valence quarks in the hadrons. This assumption is supported by the study of the pion structure function in the low x regime presented in [32]. It also gives a good description of the previous ZEUS leading neutron spectra, as shown in [10,11]. On the other hand, the direct application of (1) to HERA photoproduction data [33] leads to the result $\sigma_{\gamma\pi}^{\rm tot}/\sigma_{\gamma p}^{\rm tot}=0.32\pm0.03$, which is factor 2 lower than the ratio given above. The effective value of R_q was more recently discussed in [34] on more theoretical grounds with the conclusion that this number could reach the value of $R_q=0.5$. We shall use relation (14) to estimate $\sigma_{d\pi}$ letting R_q vary from 1/3 to 2/3.

In the eikonal approximation the dipole–proton cross section σ_{dp} is given by:

$$\sigma_{dp}(x,\boldsymbol{r})=2\int d^2\boldsymbol{b}\,\mathcal{N}^p(x,\boldsymbol{r},\boldsymbol{b})\ , \tag{15}$$

where $\mathcal{N}^p(x,\boldsymbol{r},\boldsymbol{b})$ is the imaginary part of the forward amplitude for the scattering between a small dipole (a colorless quark–antiquark pair) and a dense hadron target, at a given rapidity

interval $Y = \ln(1/x)$. The dipole has transverse size given by the vector $\boldsymbol{r} = \boldsymbol{x} - \boldsymbol{y}$, where $\boldsymbol{x}$ and $\boldsymbol{y}$ are the transverse vectors for the quark and antiquark, respectively, and impact parameter $\boldsymbol{b} = (\boldsymbol{x} + \boldsymbol{y})/2$. As mentioned in the introduction, at very high energies (and very low x) the evolution with the rapidity Y of $\mathcal{N}^p(x, \boldsymbol{r}, \boldsymbol{b})$ is given by the Balitsky–Kovchegov (BK) equation [19, 20] assuming the translational invariance approximation, which implies $\mathcal{N}^p(x, \boldsymbol{r}, \boldsymbol{b}) = \mathcal{N}^p(x, \boldsymbol{r})S(\boldsymbol{b})$ and $\sigma_{dp}(x, \boldsymbol{r}) = \sigma_0 \cdot \mathcal{N}^p(x, \boldsymbol{r})$, with the normalization of the dipole cross section (σ_0) being fitted to data. Alternatively, we can describe the scattering amplitude $\mathcal{N}^p(x, \boldsymbol{r})$ using phenomenological models based on saturation physics constructed taking into account the analytical solutions of the BK equation which are known in the low and high density regimes. The main advantage in the use of phenomenological models is that we can easily compare the linear and nonlinear predictions, which is useful to determine the contribution of the saturation effects to the process under analysis. In what follows we will consider as input the phenomenological models proposed in Refs. [35–37]. In particular, the IIMS model, proposed in Ref. [36] and updated in [37], was constructed so as to reproduce two limits of the LO BK equation analytically under control: the solution of the BFKL equation for small dipole sizes, $r \ll 1/Q_s(x)$, and the Levin–Tuchin law for larger ones, $r \gg 1/Q_s(x)$. In the updated version of this parametrization [37], the free parameters were obtained by fitting the new H1 and ZEUS data. In this parametrization the forward dipole–proton scattering amplitude is given by

$$\mathcal{N}^p(x, \boldsymbol{r}) = \begin{cases} \mathcal{N}_0 \left(\frac{r\,Q_s}{2}\right)^{2\left(\gamma_s + \frac{\ln(2/r\,Q_s)}{\kappa\,\lambda\,Y}\right)}, & \text{for } r\,Q_s(x) \leq 2\,, \\ 1 - \mathrm{e}^{-a\,\ln^2(b\,r\,Q_s)}\,, & \text{for } r\,Q_s(x) > 2\,, \end{cases} \tag{16}$$

where a and b are determined by continuity conditions at $r\,Q_s(x) = 2$, $\gamma_s = 0.7376$, $\kappa = 9.9$, $\mathcal{N}_0 = 0.7$ and Q_s is the saturation scale given by:

$$Q_s^2(x) = Q_0^2 \left(\frac{x_0}{x}\right)^{\lambda} \tag{17}$$

with $x_0 = 1.632 \times 10^{-5}$, $\lambda = 0.2197$, $Q_0^2 = 1.0$ GeV^2. The first line of Eq. (16) describes the linear regime whereas the second one includes saturation effects. In the literature there is an improved version of the IIMS model, called bCGC [38] where the scattering amplitude (16) and the saturation scale (17) depend on the impact parameter. We have used it in our calculations. The results were so close to those obtained with the IIMS, that we have decided to keep only the latter. Another well known dipole model is the GBW model [35], which captures the basic features of saturation physics and allows for simple analytical estimates. The GBW dipole–proton scattering amplitude is given by

$$\mathcal{N}^p(x, \boldsymbol{r}) = 1 - \exp\left[-\frac{Q_s^2 r^2}{4}\right] \tag{18}$$

with $Q_0^2 = 1.0$ GeV^2, $x_0 = 3 \times 10^{-4}$ and $\lambda = 0.288$. Finally, we will also use the dipole–proton cross section estimated with the help of the DGLAP analysis of the gluon distribution, which is given by [39]:

$$\sigma_{dip}(x, \boldsymbol{r}) = \frac{\pi^2}{3} r^2 \alpha_s x g(x, 10/r^2) \tag{19}$$

where $xg(x, Q^2)$ is the target gluon distribution, for which we use the CTEQ6 parametrization [40]. The above expression represents the linear regime of QCD and is a baseline for comparison with the nonlinear predictions.

3. Results

As it was seen in the previous sections, the leading neutron spectrum depends essentially on two main ingredients: the pion flux and the dipole–pion cross section. The latter is very sensitive to the value of the involved Bjorken x, or, in our case, $\hat{x}$. In Fig. 2 we show $\hat{x}$ as a function of x_L. From the figure we can conclude that at the highest values of the present photon–hadron energies (W) and at the lowest values of Q^2 we enter deeply in the low x domain. This will be even more so if measurements can be carried out at higher energies, but already at the available energies we can see that the leading neutron spectrum receives a contribution from the kinematical range where the nonlinear effects are expected to be present and hence it is interesting to investigate their influence.

We now address the dependence of our predictions for the leading neutron spectra on the models of the pion flux and of the dipole–pion scattering amplitude. In Fig. 3 (a) we show the different parametrizations of the pion flux introduced in the previous section as a function of x_L. In Fig. 3 (b) we show several dipole pion cross sections as a function of x_L. From the figure we can see that in the low x_L region the spread between the different curves is wider. Moreover, from Fig. 2 we can see that in the low x_L region we move to the low $\hat{x}$ domain, where saturation effects become more pronounced. Data points in this region are thus crucial to discriminate between models.

It is important to emphasize that the spectrum is proportional to the product of the pion flux and the dipole–pion scattering amplitude. Consequently, in what follows we will initially assume a given model for one of these quantities and analyze the dependence on the other quantity. Having done that, we will choose one combination, calculate the normalized cross section $(1/\sigma_{DIS})d\sigma/dx_L$ and compare with the experimental data. The normalization was taken from Ref. [41] and is given by:

$$\sigma_{DIS} = \frac{4\pi^2 \alpha_{em}}{Q^2} \frac{c}{x^{\beta}} \tag{20}$$

where $c = 0.18$, $\beta = d\,\ln(Q^2/\Lambda_0^2)$ with $d = 0.0481$ and $\Lambda_0 = 0.292$ GeV.

In Fig. 4 (a) we consider the IIMS model for the scattering amplitude and estimate the leading neutron spectrum using the different models of the pion flux discussed in the previous section. We observe that the behavior at medium and small values of x_L is strongly dependent on the choice of the model. Using the cut-off Λ_c in the range defined in Ref. [16], our results suggest that model f_6 is disfavored. In our analysis we have considered all the pion fluxes which have been previously used by the experimental groups [2] to describe their data. Up to now there are still too many theoretical uncertainties to attempt an ultimate fit of the leading neutron spectra, determining unambiguously the best pion flux. Nevertheless, we can say that, in comparison to the other models, the f_2 model has one interesting feature which is its long and comparatively flat tail in the low x_L region, which makes possible a fit of the data in this region even without including a contribution from other processes. The other models fall too quickly at low x_L and this cannot be easily cured just by changing the values of Q^2, the factor K or the factor R_q. However, the subleading contributions mentioned above are more important in the low x_L region of the spectrum and their inclusion combined with other pion fluxes such as f_1 or f_3 might result in a good fit of the data as well. In view of this slight superiority of f_2, we shall use it in the remainder of this section. In Fig. 4 (b) we consider the f_2 model for the pion flux and estimate the spectra using different models of the scattering amplitude. We can see that the predictions have similar behavior in the transition between the small

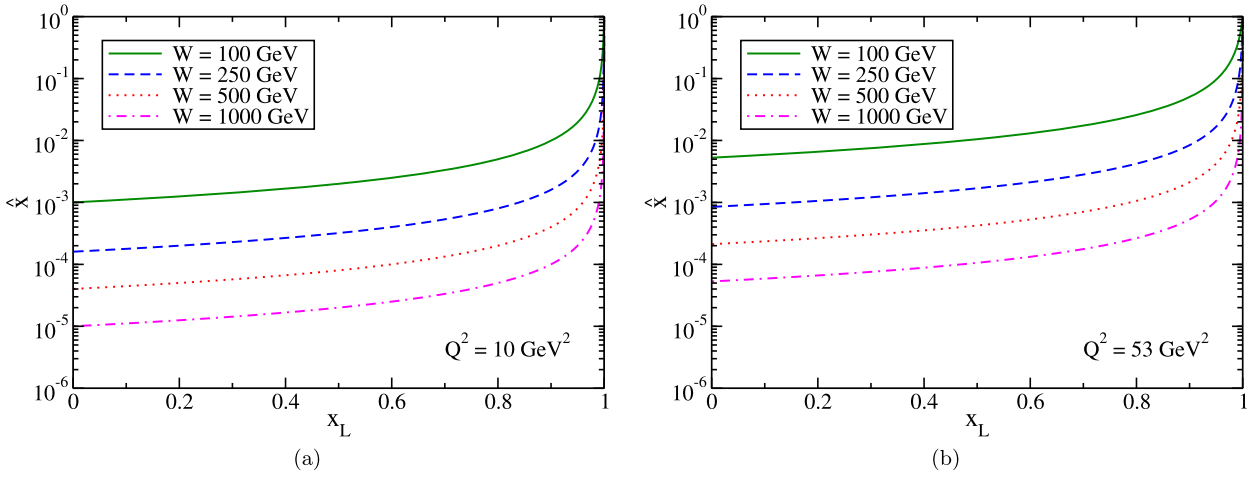

Fig. 2. Scaled Bjorken variable $\hat{x}$, (Eq. (11)), as a function of x_L for two different virtualities: (a) $Q^2 = 10$ GeV^2 and (b) $Q^2 = 53$ GeV^2.

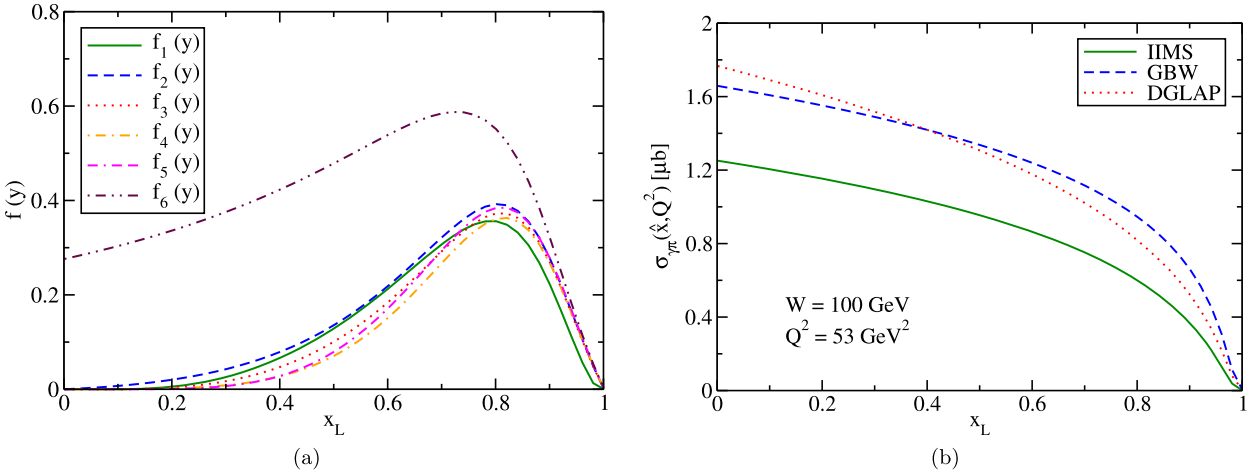

Fig. 3. a) Pion flux as a function of x_L. b) Dipole–pion cross section as a function of x_L.

and large-x_L regimes, but with the magnitude being dependent on the description of the QCD dynamics. In doing the theoretical calculations we need to work with a fixed value of Q^2. However the data are given in such a way that for each value of x_L there is a particular range of Q^2 values. We necessarily need to make a choice and we have taken the central value $Q^2 = 53$ GeV^2 in the range covered by the experiment. In order to estimate the uncertainty present in this choice, in Fig. 4 (c) we consider the f_2 and IIMS models and calculate the spectrum for different values of the photon virtuality. We observe that our predictions are more compatible with the experimental data if larger values of Q^2 are assumed.

So far we have assumed that the photon hits only the pion, in a type of "impulse approximation". However it has been shown in [10,11,13,26] that very often the photon hits also the neutron, specially in the low Q^2 domain, where the photon has low resolving power. In these cases the extra interactions generate the so called absorptive corrections, which can be estimated with models. In the case of leading neutron production, in [26] and in [13] the authors concluded that the corrections are not very large and affect almost uniformly all the x_L spectrum. On the other hand, other calculations [10,11,34,42] found a strong reduction by about a factor 2 in the cross section. In what follows we shall include the effect of absorptive corrections multiplying our spectra by a constant (independent of x_L) factor K which can assume values from 0.5 to 1.

In Fig. 5 we give our description of data. All the parameters contained in the IIMS dipole cross section have been already fixed by the analysis of other DIS data from HERA. The f_2 pion flux has been fixed by fitting previous data on leading neutron spectra. The bands account for the uncertainty in the choice of the factors R_q and K. The upper limit of each band corresponds to the choice $R_q = 2/3$ and $K = 1$ whereas the lower limit corresponds to the choice $R_q = 1/3$ and $K = 0.5$. The central dashed lines represent the choice where $R_q.K = 0.5$, which could, for example, be realized with $R_q = 0.5$ and $K = 1$. Our results follow the trend dictated by data. For now, it is not possible to be very precise. With a combined analysis of other data on exclusive production with tagged leading neutrons we hope to reduce the bands.

Finally, we analyze the Feynman scaling in leading neutron spectra and the contribution of nonlinear effects to this process. As mentioned before this process is surprisingly sensitive to low x physics. In particular, at large x_L we observe the transition from the large to small x domain. It is therefore interesting to check whether gluon saturation effects are already playing a significant role. As it can be seen from Eqs. (1) and (10), all the energy dependence is contained in the dipole forward scattering amplitude $\mathcal{N}$. Therefore, we can estimate the contribution of the nonlinear effects comparing the results obtained with saturation model, e.g. the IIMS model given in (16), with those obtained with the linear model, Eq. (19). Moreover, the theoretical expectation can be ob-

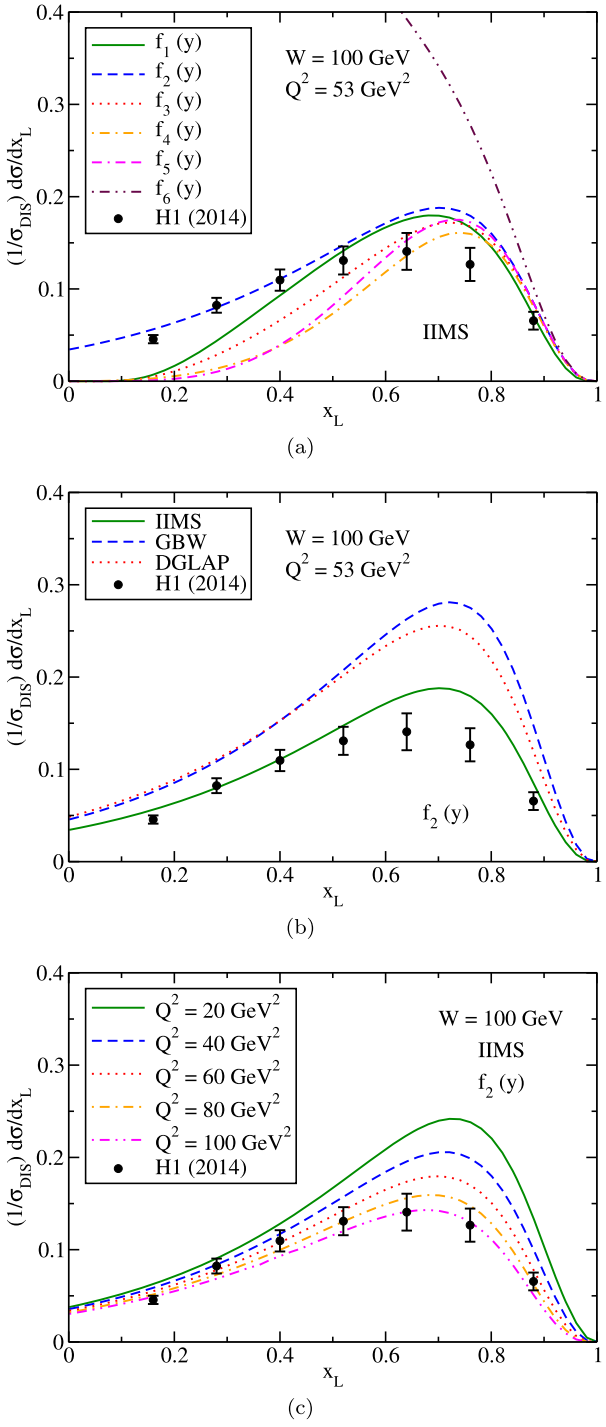

Fig. 4. Leading neutron spectra compared with experimental data at $W = 100$ GeV considering (a) the IIMS scattering amplitude and different choices of the pion flux ($Q^2 = 53$ GeV^2); (b) the f_2 pion flux and different choices for the scattering amplitude ($Q^2 = 53$ GeV^2); and (c) the f_2 pion flux and the IIMS scattering amplitude for different values of photon virtuality Q^2.

tained using the GBW model for the scattering amplitude, Eq. (18). In the linear limit, when the dipole radius is very small (or equivalently Q^2 is very large) or the saturation scale is very small (and hence the energy is not very high), we can expand the exponent and obtain

$$\sigma_{d\pi}(r,\hat{x}) \propto \sigma_0 \mathcal{N}(r,\hat{x}) \simeq \sigma_0 \frac{Q_s^2(\hat{x}) r^2}{4}$$

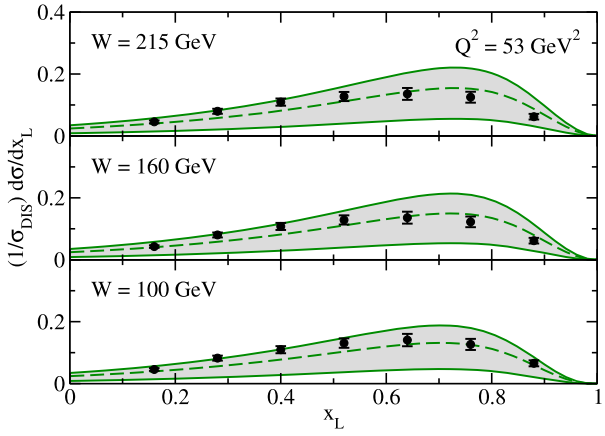

Fig. 5. Leading neutron x_L spectrum for three photon–proton energies compared with recent H1 data.

$$\simeq \sigma_0\, Q_0^2\, x_0{}^{\lambda} \left[\frac{(1-x_L)W^2 + Q^2}{Q^2 + m_f^2}\right]^{\lambda}. \tag{21}$$

Consequently, in this regime we see that the leading neutron x_L spectrum will depend on W. In a complementary way, in the nonlinear limit, when the dipole radius is very large (or equivalently Q^2 is very small) or the saturation scale is very large (and hence the energy is very high), we obtain

$$\sigma_{d\pi}(r,\hat{x}) \propto \sigma_0 \mathcal{N}(r,\hat{x}) \simeq \sigma_0 \tag{22}$$

which is energy independent. One could argue that the mere inspection of Eq. (1) would suggest that at some asymptotically high energy the photon–pion cross section would reach some "black disk" limit and the energy dependence would disappear. We would like to emphasize that the information contained in (21) and (22) is much richer and indicates the route through which the asymptotic limit is reached and the role played by nonlinear effects. These expectations can be compared with those obtained using the IIMS and DGLAP models for the dipole–pion cross section. In Fig. 6 (a) we show the spectra obtained in a purely linear approach. As expected we see a noticeable energy dependence. In contrast, the nonlinear predictions presented in Fig. 6 (b) show a remarkable suppression of the energy dependence at low values of Q^2, consistent with the expectations. These results indicate that the Feynman scaling (and how it is violated) can be directly related to the QCD dynamics at small-x.

We close this section, emphasizing that, in order to study Feynman scaling it is desirable to have data at high energies, in the very forward neutron rapidity region (large x_L) and at a fixed value of Q^2. The onset of saturation effects happens when $Q^2 < Q_s^2$, where Q_s is the saturation scale given by Eq. (17). It is difficult to be very precise, but from the curves shown in Fig. 6 (b) and from the accumulated experience with high energy processes, it is reasonable to say that saturation (and hence Feynman scaling) would be visible at $Q^2 \simeq 1 - 2$ GeV^2.

4. Summary

In this work we have studied leading neutron production in $e + p \to e + n + X$ collisions at high energies and have calculated the Feynman x_L distribution of these neutrons. The differential cross section was written in terms of the pion flux and the photon–pion total cross section. We have proposed to describe this process using the color dipole formalism and, assuming the validity of the additive quark model, we have related the dipole–pion with the well determined dipole–proton cross section. In this

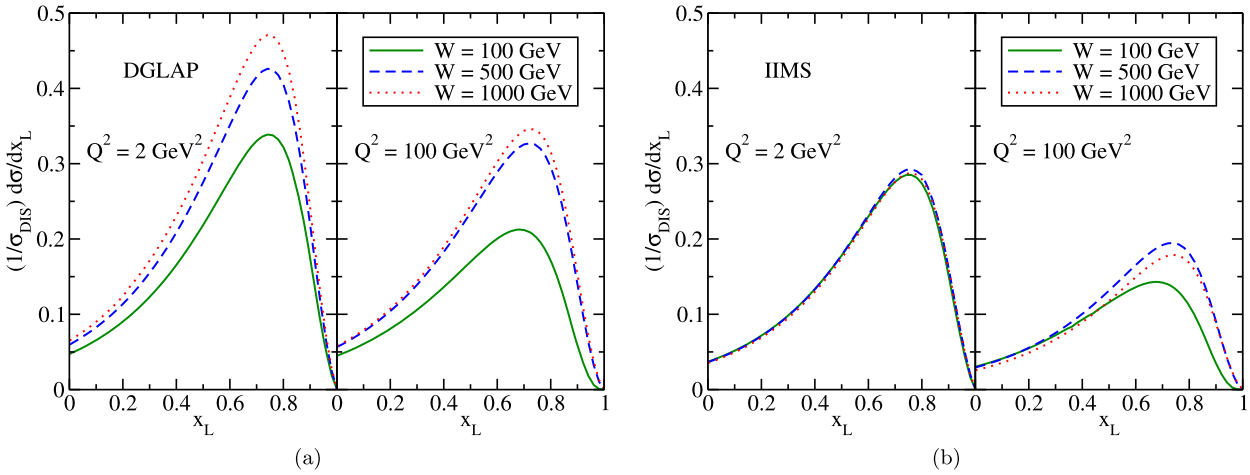

Fig. 6. (a) Leading neutron spectra for different energies considering (a) the linear DGLAP model and (b) the nonlinear IIMS model for the dipole–pion cross section.

formalism we have been able to estimate the dependence of the predictions on the description of the QCD dynamics at high energies as well as the contribution of gluon saturation effects to leading neutron production. With the parameters constrained by other phenomenological information, we were able to reproduce the basic features of the recently released H1 leading neutron spectra. Presenting an ultimate fit of these data is a difficult and still open problem, which we do not try to solve in this paper. We just wanted to include a new ingredient in the theoretical framework: saturation physics, implemented via color dipole models. After introducing the idea, the calculation just aimed at showing that the description of leading neutron spectra using (among other ingredients) saturation models is compatible with data, not in conflict with them. After illustrating this compatibility, the next step would have been to produce the most complete fit of data, possibly excluding flux factors and/or dipole cross sections. Unfortunately, this is not yet possible, because so far there are too many uncertainties in the calculation. The sources of these uncertainties in the computation of leading neutron spectra are: i) the strength of the absorptive corrections represented by the factor K; ii) the strength of the sub-leading contributions, such ρ and a_2 emission; iii) the validity of the additive quark model for the photon–pion cross section represented by the factor R_q; iv) the precise knowledge of Q^2 to be used in the calculations; v) the strength of the contribution from direct fragmentation of the proton into neutrons (estimated in the Monte Carlo simulations in the Ref. [1]); vi) the precise form of the pion flux; vii) the precise form of the dipole cross section.

It may be possible to constrain the unknown numbers and assumptions with the help of more experimental data on exclusive processes with tagged leading neutrons, such as those on D^* production [2] and those on ρ production, released very recently by the H1 Collaboration [43]. Work along this line is in progress. Finally, one of our most interesting conclusions is that leading neutron spectra can be used to probe the low x content of the pion target and hence it is a new observable where we can look for gluon saturation effects. At higher energies this statement will become more valid. Moreover saturation physics provides a precise route to Feynman scaling, which will eventually happen at higher energies.

Acknowledgements

We are deeply grateful to W. Melnitchouk, to C.R. Ji and to B. Kopeliovich for enlightening discussions. This work was partially financed by the Brazilian funding agencies CNPq, CAPES, FAPERGS and FAPESP.

References

[1] D.S. Barton, et al., Phys. Rev. D 27 (1982) 2580;
A.E. Brenner, et al., Phys. Rev. D 26 (1982) 1497;
EHS/NA22 Collaboration, N.M. Agababyan, et al., Z. Phys. C 75 (1996) 229;
N. Cartiglia, AIP Conf. Proc. 407 (1997) 515;
S. Chekanov, et al., ZEUS Collaboration, Nucl. Phys. B 776 (2007) 1.
[2] S. Chekanov, et al., ZEUS Collaboration, Phys. Lett. B 590 (2004) 143.
[3] J. Olsson, H1 Collaboration, PoS DIS 2014 (2014) 156;
V. Andreev, et al., H1 Collaboration, Eur. Phys. J. C 74 (2014) 2915;
F.D. Aaron, et al., H1 Collaboration, Eur. Phys. J. C 68 (2010) 381.
[4] M. Bishari, Phys. Lett. B 38 (1972) 510.
[5] H. Holtmann, et al., Phys. Lett. B 338 (1994) 363.
[6] B. Kopeliovich, B. Povh, I. Potashnikova, Z. Phys. C 73 (1996) 125.
[7] S. Kumano, Phys. Rev. D 43 (1991) 59.
[8] N.N. Nikolaev, et al., Phys. Rev. D 60 (1999) 014004.
[9] L.L. Frankfurt, L. Mankiewicz, M.I. Strikman, Z. Phys. A 334 (1989) 343;
T.T. Chou, C.N. Yang, Phys. Rev. D 50 (1994) 590;
K. Golec-Biernat, J. Kwiecinski, A. Szczurek, Phys. Rev. D 56 (1997) 3955;
M. Przybycien, A. Szczurek, G. Ingelman, Z. Phys. C 74 (1997) 509;
W. Melnitchouk, J. Speth, A.W. Thomas, Phys. Rev. D 59 (1998) 014033;
A. Szczurek, N.N. Nikolaev, J. Speth, Phys. Lett. B 428 (1998) 383.
[10] A.B. Kaidalov, V.A. Khoze, A.D. Martin, M.G. Ryskin, Eur. Phys. J. C 47 (2006) 385.
[11] V.A. Khoze, A.D. Martin, M.G. Ryskin, Eur. Phys. J. C 48 (2006) 797.
[12] N.N. Nikolaev, J. Speth, B.G. Zakharov, arXiv:hep-ph/9708290.
[13] U. D'Alesio, H.J. Pirner, Eur. Phys. J. A 7 (2000) 109.
[14] See, for example ZEUS Collaboration, M. Derrick, et al., Phys. Lett. B 384 (1996) 388.
[15] M. Burkardt, K.S. Hendricks, C.R. Ji, W. Melnitchouk, A.W. Thomas, Phys. Rev. D 87 (2013) 056009.
[16] Y. Salamu, C.R. Ji, W. Melnitchouk, P. Wang, Phys. Rev. Lett. 114 (2015) 122001.
[17] F. Gelis, E. Iancu, J. Jalilian-Marian, R. Venugopalan, Annu. Rev. Nucl. Part. Sci. 60 (2010) 463;
E. Iancu, R. Venugopalan, arXiv:hep-ph/0303204;
H. Weigert, Prog. Part. Nucl. Phys. 55 (2005) 461;
J. Jalilian-Marian, Y.V. Kovchegov, Prog. Part. Nucl. Phys. 56 (2006) 104;
J.L. Albacete, C. Marquet, Prog. Part. Nucl. Phys. 76 (2014) 1.
[18] J. Jalilian-Marian, A. Kovner, L. McLerran, H. Weigert, Phys. Rev. D 55 (1997) 5414;
J. Jalilian-Marian, A. Kovner, H. Weigert, Phys. Rev. D 59 (1999) 014014;
J. Jalilian-Marian, A. Kovner, H. Weigert, Phys. Rev. D 59 (1999) 014015;
J. Jalilian-Marian, A. Kovner, H. Weigert, Phys. Rev. D 59 (1999) 034007;
A. Kovner, J. Guilherme Milhano, H. Weigert, Phys. Rev. D 62 (2000) 114005;
H. Weigert, Nucl. Phys. A 703 (2002) 823;
E. Iancu, A. Leonidov, L. McLerran, Nucl. Phys. A 692 (2001) 583;
E. Ferreiro, E. Iancu, A. Leonidov, L. McLerran, Nucl. Phys. A 701 (2002) 489.
[19] I.I. Balitsky, Phys. Rev. Lett. 81 (1998) 2024;
I.I. Balitsky, Phys. Lett. B 518 (2001) 235;
I.I. Balitsky, A.V. Belitsky, Nucl. Phys. B 629 (2002) 290.
[20] Y.V. Kovchegov, Phys. Rev. D 60 (1999) 034008;
Y.V. Kovchegov, Phys. Rev. D 61 (2000) 074018.
[21] T. Sako, LHCf Collaboration, arXiv:1010.0195 [hep-ex].
[22] O. Adriani, L. Bonechi, M. Bongi, G. Castellini, R. D'Alessandro, A. Faus, K. Fukatsu, M. Haguenauer, et al., Nucl. Phys. Proc. Suppl. 212 (2011) 270.

[23] Y. Itow, H. Menjo, G. Mitsuka, T. Sako, K. Kasahara, T. Suzuki, S. Torii, O. Adriani, et al., arXiv:1401.1004 [physics.ins-det];
Y. Itow, H. Menjo, T. Sako, N. Sakurai, K. Kasahara, T. Suzuki, S. Torii, O. Adriani, et al., arXiv:1409.4860 [physics.ins-det];
L. Bonechi, O. Adriani, E. Berti, M. Bongi, G. Castellini, R. D'Alessandro, M. Del Prete, M. Haguenauer, et al., EPJ Web Conf. 71 (2014) 00019.
[24] J.D. Sullivan, Phys. Rev. D 5 (1972) 1732;
A.W. Thomas, Phys. Lett. B 126 (1983) 97.
[25] W. Melnitchouk, M. Malheiro, Phys. Rev. C 55 (1997) 431;
J. Speth, A.W. Thomas, Adv. Nucl. Phys. 24 (1998) 83;
S. Kumano, Phys. Rep. 303 (1998) 183;
H. Holtmann, A. Szczurek, J. Speth, Nucl. Phys. A 569 (1996) 631.
[26] N.N. Nikolaev, W. Schaefer, A. Szczurek, J. Speth, Phys. Rev. D 60 (1999) 014004.
[27] F.S. Navarra, M. Nielsen, C.A.A. Nunes, M. Teixeira, Phys. Rev. D 54 (1996) 842;
S. Paiva, M. Nielsen, F.S. Navarra, F.O. Durães, L.L. Barz, Mod. Phys. Lett. A 13 (1998) 2715;
W. Melnitchouk, A.W. Thomas, Phys. Lett. B 414 (1997) 134.
[28] S.J. Brodsky, B.Q. Ma, Phys. Lett. B 381 (1996) 317.
[29] E.A. Hawker, et al., E866/NuSea Collaboration, Phys. Rev. Lett. 80 (1998) 3715.
[30] F. Carvalho, F.O. Duraes, F.S. Navarra, M. Nielsen, F.M. Steffens, Eur. Phys. J. C 18 (2000) 127.
[31] A.W. Thomas, C. Boros, Eur. Phys. J. C 9 (1999) 267.
[32] N.N. Nikolaev, J. Speth, V.R. Zoller, Phys. Lett. B 473 (2000) 157.
[33] S. Chekanov, et al., ZEUS Collaboration, Nucl. Phys. B 637 (2002) 3.
[34] B.Z. Kopeliovich, I.K. Potashnikova, B. Povh, I. Schmidt, Phys. Rev. D 85 (2012) 114025.
[35] K.J. Golec-Biernat, M. Wusthoff, Phys. Rev. D 59 (1998) 014017.
[36] E. Iancu, K. Itakura, S. Munier, Phys. Lett. B 590 (2004) 199.
[37] G. Soyez, Phys. Lett. B 655 (2007) 32.
[38] H. Kowalski, L. Motyka, G. Watt, Phys. Rev. D 74 (2006) 074016;
G. Watt, H. Kowalski, Phys. Rev. D 78 (2008) 014016.
[39] V. Barone, E. Predazzi, High-Energy Particle Diffraction, Springer-Verlag, Berlin, Heidelberg, 2002;
E. Iancu, A.H. Mueller, Nucl. Phys. A 730 (2004) 460;
G.P. Salam, Nucl. Phys. B 461 (1996) 512.
[40] H.L. Lai, J. Huston, Z. Li, P. Nadolsky, J. Pumplin, D. Stump, C.-P. Yuan, Phys. Rev. D 82 (2010) 054021.
[41] C. Adloff, et al., Phys. Lett. B 520 (2001) 183.
[42] B.Z. Kopeliovich, I.K. Potashnikova, I. Schmidt, J. Soffer, Phys. Rev. D 78 (2008) 014031.
[43] V. Andreev, et al., H1 Collaboration, arXiv:1508.03176 [hep-ex].